

# Effect of Dy<sup>3+</sup> on the physical, optical and radiative properties of CaSO<sub>4</sub>–B<sub>2</sub>O<sub>3</sub>–P<sub>2</sub>O<sub>5</sub> glasses

Y A Yamusa<sup>1,2\*</sup>, R Hussin<sup>1</sup> and W N W Shamsuri<sup>1</sup>

<sup>1</sup>Department of Physics, Faculty of Science, Universiti Teknologi Malaysia, 81310 Skudai, Johor, Malaysia

<sup>2</sup>Centre for Energy Research and Training, Ahmadu Bello University, Zaria 1014, Kaduna State, Nigeria

Received: 08 November 2017 / Accepted: 17 May 2018 / Published online: 17 August 2018

**Abstract:** The unprecedented attributes of the trivalent rare earth ions-doped sulfoborophosphate glasses have led to tremendous interest in exploring their potentials for application in diverse photonic devices. Calcium sulfoborophosphate glasses doped with dysprosium ions were prepared by a melt-quenching technique with varying concentrations of Dy<sup>3+</sup> that range from 0.1 to 1.0 mol%. Amorphous nature of the prepared glasses was determined using X-ray diffraction, while the presence of BO<sub>3</sub>, BO<sub>4</sub>, P–O–P, PO<sub>4</sub>, P–O–B, O–P–O, SO<sub>4</sub> and B–O–B units was determined via FTIR study. Glass density and molar volume were found to be between 2.203 to 2.222 g cm<sup>-3</sup> and 48.10 to 48.80 m<sup>3</sup> mol<sup>-1</sup>, respectively. The direct and indirect bandgap and Urbach's energy were found to be within 4.183–4.312 eV, 3.423–3.718 eV and 0.381–0.447 eV energy ranges, respectively. The absorption spectra displayed nine prominent peaks centered at 351, 383, 451, 752, 799, 896, 1090, 1269 and 1670 nm corresponding to <sup>6</sup>H<sub>15/2</sub> → <sup>6</sup>P<sub>7/2</sub>, <sup>4</sup>F<sub>7/2</sub>, <sup>4</sup>I<sub>15/2</sub>, <sup>6</sup>F<sub>3/2</sub>, <sup>6</sup>F<sub>5/2</sub>, <sup>6</sup>F<sub>7/2</sub>, <sup>6</sup>F<sub>9/2</sub>, <sup>6</sup>H<sub>11/2</sub> and <sup>6</sup>H<sub>13/2</sub> transitions. The emission spectrum of calcium sulfoborophosphate glasses doped with Dy<sup>3+</sup> shows two prominent bands at 482 nm (<sup>4</sup>F<sub>9/2</sub> → <sup>6</sup>H<sub>15/2</sub>) and 572 nm (<sup>4</sup>F<sub>9/2</sub> → <sup>6</sup>H<sub>13/2</sub>) and two weak bands at 661 nm (<sup>4</sup>F<sub>9/2</sub> → <sup>6</sup>H<sub>11/2</sub>) and 684 nm (<sup>4</sup>F<sub>9/2</sub> → <sup>6</sup>H<sub>9/2</sub>) under 345 nm excitation. The calculated bonding parameters (δ) were found to be ionic in nature. Judd–Ofelt parameters Ω<sub>λ</sub> (λ = 2, 4 and 6) have been calculated from the absorption spectra. The emission cross sections, as well as the branching ratios for two intense emission transitions <sup>4</sup>F<sub>9/2</sub> → <sup>6</sup>H<sub>15/2</sub> and <sup>4</sup>F<sub>9/2</sub> → <sup>6</sup>H<sub>13/2</sub>, have been calculated. The excellent features demonstrated by the present glasses amplify their suitability for solid-state lasers, nonlinear optical and white LEDs applications.

**Keywords:** Sulfoborophosphate glasses; FTIR; Optical and radiative properties; Judd–Ofelt theory; Dysprosium ions

**PACS No.:** 78.66.Jg

## 1. Introduction

The excellent spectroscopic properties of rare earth (RE) ion-doped glasses in the formulation of novel optical devices such as solid-state lasers, optical communication fibers, sensors and light converters have recently engrossed considerable attention [1]. Detailed radiative properties of rare earth ions in glasses could be identified via optical characteristics determination. However, it depends on the network matrix and appropriate choice of host forming and network modifying ions [2]. Also, dysprosium ions have been efficaciously added into several glasses, obtaining two

intense emissions associated with the blue and yellow luminescence material. White light can be produced when these two principal emissions are combined. Among different optical materials fitting the oxide glass household, the fundamental P<sub>2</sub>O<sub>5</sub> multi-component glass arrangement exhibits numerous benefits for potential application in optical devices design [3, 4].

Rare earth ion-doped glasses whose emission characteristics fall within the mid-infrared wavelength (2–5 μm) are found to be useful in the design of compact microchip lasers, planar waveguides and display devices [5]. The dysprosium ions-doped glasses are widely examined in telecommunication for the formation of optical amplifier systems. The dysprosium ions give two distinctive emission transitions that correspond to <sup>4</sup>F<sub>9/2</sub> → <sup>6</sup>H<sub>15/2</sub> in blue

\*Corresponding author, E-mail: yamusaabdullahi@yahoo.com

(486 nm) and  ${}^4F_{9/2} \rightarrow {}^6H_{13/2}$  in yellow (577 nm) region and are used for white-light-emitting phosphors [6]. Furthermore, the  ${}^4F_{9/2} \rightarrow {}^6H_{15/2}$  transition is less sensitive to the host, whereas the  ${}^4F_{9/2} \rightarrow {}^6H_{13/2}$  transition is hypersensitive and therefore its intensity strongly depends on the host [7].

Phosphate glasses have several characteristics of commercial applications due to their softening temperatures, low melting, high thermal expansion coefficients, optical characteristics and high electrical conductivity [8]. Borate-based glasses have fascinating optical and structural properties.  $BO_4$  tetrahedral and  $BO_3$  triangle borate glass structure is not a random distribution; rather, it is a three-dimensional random glass network that gives a definite and stable borate groups such as tetraborates, diborates and triborates. [9]. These structural modifications of the glass structure typically occur due to the conditions applied during glass preparation and involvement of several types of modifiers during the selection of chemical composition. Phosphate and borate glasses have gained more attention from researchers over the decades [10–12] due to their brittle physical and structural properties [13–15]. However, both phosphate and borate glasses have certain weaknesses, which are the hygroscopic nature of phosphate glass and the structural instability of borate glass [16]. Hence, both phosphate and borate glass systems have low chemical durability [17].

The overwhelming potentials of phosphate and borate glasses that have drawn the attention of researchers, particularly in sulfoborophosphate glasses, include good transparency from the ultraviolet to the near-infrared regions, excellent optical properties, low dispersion and low refractive indices [8]. The existence of borate in phosphate glass enhances the chemical durability due to the presence of boron oxide composition in the structural network, typically in the form of  $BO_4$  tetrahedral, which transmutes metaphosphate chain into a three-dimensional network [8]. Sulfoborophosphate glasses, when imbedded with alkaline earth ions, are said to possess numerous properties that make them suitable for essential applications such as phosphors, radiation dosimetry, solar energy converters, semiconductors lithography and vacuum ultraviolet (VUV) optics.

This study was aimed to synthesize sulfoborophosphate glasses doped with  $Dy^{3+}$  ions and examine their structural properties by varying the rare earth ion content. The compositional roles of  $CaSO_4$ – $B_2O_3$ – $P_2O_5$  glasses doped with dysprosium ions on their optical and physical properties were assessed. Radiative transition probability, fluorescence branching ratio and emission cross section were calculated using the so-called Judd–Ofelt theory. Photoluminescence spectra resulting in good fabrication of new

solid-state laser devices were analyzed and compared with the existing reported work.

## 2. Materials and methods

### 2.1. Sample preparation

Calcium sulfoborophosphate glass sample doped with  $Dy^{3+}$  with different compositions of  $25CaSO_4$ – $30B_2O_3$ – $(45-x)P_2O_5$ – $x Dy_2O_3$  (where  $x = 0.1, 0.3, 0.5, 0.7$  and  $1.0$  mol%) was prepared by a melt-quenching technique. The imported pure chemicals of high-purity glass constituents (99.99%, Sigma-Aldrich) used in this work were calcium sulfate ( $CaSO_4$ ), Boric acid ( $H_3BO_3$ ), phosphoric acid ( $H_3PO_4$ ) and dysprosium oxide ( $Dy_2O_3$ ) of about 30 g, which were accurately weighed using a standard analytical balance. The samples were mixed using alumina crucible and then kept in an electric furnace, preheated at  $200^\circ C$  for 30 min to eliminate the  $H_2O$  and  $H_2S$  content and subsequently heated at  $1300^\circ C$  for 1 h. The glass samples prepared by a melt-quenching technique were air quenched by transferring them into a preheated stainless steel mold, kept for annealing at  $300^\circ C$  for 3 h to remove thermal strains and then gradually allowed to cool to room temperature. Then, the glass samples were polished to their flat surfaces for transparency and further characterization.

### 2.2. Parameters of the instrumentations

#### 2.2.1. X-ray diffraction

The amorphous state of the prepared glass samples was assessed by X-ray diffraction using a Bruker D8 Advance diffractometer employing  $Cu$ – $K\alpha$  radiations ( $\lambda = 1.54 \text{ \AA}$ ) functioning at the rate of 100 mA and 40 kV. The diffraction shapes of the prepared samples were used at a scanning rate of  $0.05^\circ/s$  and recorded in the range of  $2\theta = 0^\circ$ – $100^\circ$ .

#### 2.2.2. Fourier transform infrared

The spectral range of  $400$ – $2400 \text{ cm}^{-1}$  was used to record the Fourier transform infrared transmissions. A PerkinElmer FTIR 1660 spectrometer was used for the measurement. KBr at a ratio of 1:100 and comparatively fine glass powder were mixed, and transparent pellets of each sample were formed.

#### 2.2.3. UV–Vis–NIR spectroscopic

The near-ultraviolet and visible regions were recorded by a bulk form of the samples, and their spectral measurement

was assessed with a thin film at the Department of Physics, Universiti Teknologi Malaysia. The spectrophotometer results were revealed at the range of 300–2100 nm with a photomultiplier R-928 and a double monochromatic diffraction grating system.

**2.2.3.1. Optical bandgap and Urbach's energy** Davis and Mott [18] formulated the relation between absorption coefficient ( $\alpha$ ) and photon energy ( $h\nu$ ) of the incident radiation for direct and indirect optical energy bandgap ( $E_g$ ), which can be found from Tauc's plot using

$$\alpha h\nu = B(h\nu - E_g)^n, \quad (1)$$

where  $B$  is a constant called band tailing parameter and  $n = 2$  for direct allowed,  $n = 1/2$  for indirect allowed,  $n = 3$  for direct forbidden and  $n = 1/3$  for indirect forbidden. The Urbach's energy is calculated using

$$\ln \alpha = \frac{h\nu}{E_{urb}} - c. \quad (2)$$

Equation 2 can be expressed in the form of  $y = mx + c$ , where  $m$  signifies the slope and  $c$  is constant (intercept). Therefore, Urbach's energy ( $E_{urb}$ ) is deduced as the inverse of the slope from the plot of  $\ln \alpha$  versus photon energy.

**2.2.3.2. Refractive index and electronic polarizability** Refractive index and molar refraction are important properties in optical glasses, and they have close connection with polarization properties. Therefore, the refractive index ( $n$ ) of glass in terms of optical bandgap ( $E_{opt}$ ) could be calculated from

$$\frac{(n^2 - 1)}{(n^2 + 2)} = 1 - \left(\frac{E_{opt}}{20}\right)^{1/2}. \quad (3)$$

The relationship between refractive index to molar refraction and molar volume of a glass is defined by the Lorentz–Lorenz equation and can be expressed as

$$R_m = \left(\frac{n^2 - 1}{n^2 + 2}\right) V_m, \quad (4)$$

where  $R_m$  is the molar refraction,  $n$  is the linear refractive index and  $V_m$  is the molar volume. This relationship gives the average value of molar refraction for isotopic substances such as glasses and polycrystalline materials [19]. The glass structural material is related to the molar refraction by introducing the Avogadro's number into the equation

$$\alpha_m = \left(\frac{3}{\pi N_A}\right) R_m. \quad (5)$$

The electronic polarizability is based on the magnitude of electrons' responses to an electric field denoted by the

Lorentz–Lorenz equation with  $\alpha_m$  in ( $\text{\AA}$ ). Therefore, the above expression can be rewritten as  $\alpha_m = R_m/2.52$ . Furthermore, other important parameters could be evaluated from the value of the refractive index as follows: dielectric constant  $\epsilon = n^2$ , optical dielectric constant  $\epsilon = n^2 - 1$  and reflection loss from the glass surface  $= (n - 1/n + 1)^2$ .

#### 2.2.4. Photoluminescence spectra

Wavelength of 300–1800 nm at room temperature using a Shimadzu 3101 UV–Vis–NIR spectrophotometer was used to determine the absorption spectra. PerkinElmer LS55 luminescence spectrophotometer was used to examine and record the excitation and emission spectra at a resolution of  $\pm 0.1$  nm. Excitation of the prepared samples was achieved by means of xenon discharge lamp in the range of 200 nm  $< \lambda < 900$  nm. Monk–Gillieson monochromator photodiode detector was used to determine the luminescence signal at precise excitation wavelength.

#### 2.2.5. Density and molar volume

The density ( $\rho$ ) of the prepared glass samples with an error of  $\pm 0.001$  g cm<sup>-3</sup> was measured by Archimedes principle (analytical balance of specific density—Precisa XT220A). The density of each sample was calculated using the expression

$$\rho = \frac{a}{a - b} \rho_x, \quad (6)$$

where  $a$  is the weight of the glass sample in air,  $b$  is the weight of the glass sample in toluene that was used as an immersion fluid and  $\rho_x = 0.866$  g cm<sup>-3</sup> = toluene. Then, the molar volume  $V_m$  was evaluated from the relation

$$V_m = \frac{M}{\rho} (\text{cm}^3 \text{ mol}^{-1}), \quad (7)$$

where  $V_m$  is the molar volume,  $M$  is the molecular weight and  $\rho$  is the density.

#### 2.2.6. Ion concentration and polaron radius

The ion concentration and polaron radius of the dopant (Dy<sup>3+</sup>) in the glass samples could be calculated by the expressions

$$N_i = \frac{N\rho X}{M_{av}}, \quad (8)$$

$$r_p(\text{\AA}) = \frac{1}{2} \left(\frac{\pi}{6N_i}\right)^{1/3}, \quad (9)$$

where  $N$  is the Avogadro's number,  $\rho$  is the density of the glass,  $X$  is the mole fraction of dopant in mol% and  $M_{av}$  is

the molecular weight of the sample. Two other related important properties could be evaluated after finding the value of ion concentration according to Lai et al. [20]. These parameters are as follows: field strength =  $Z/r_p^2$  and inter-nuclear distance =  $r_i$  (Å) =  $(1/N_i)^{1/3}$ , where  $Z$  is the atomic number of the dopant.

The experimental oscillator strength of lanthanide ion-doped glasses can be determined by measuring the area under the absorption bands and can be calculated using the formula [21]

$$f_{\text{exp}} = \frac{2303mc^2}{N_A\pi e^2} \int \varepsilon(\nu) d\nu = 4.32 \times 10^{-9} \int \varepsilon(\nu) d\nu, \quad (10)$$

where  $m$  is the mass of the electron,  $c$  is the speed of light,  $N_A$  is the Avogadro's number,  $e$  is the charge of an electron and  $\varepsilon(\nu)$  is the molar absorption coefficient of a band at a wavenumber  $\nu$  ( $\text{cm}^{-1}$ ).  $\varepsilon(\nu)$  is obtained from Beer–Lambert's law and can be expressed as:

$$\varepsilon(\nu) = \frac{1}{cl} \log\left(\frac{I_0}{I}\right), \quad (11)$$

where  $c$  is the concentration of rare earth ions in mol/l,  $l$  is the thickness of the sample in cm and  $\log\left(\frac{I_0}{I}\right)$  is the optical density in wavenumber,  $\nu$  ( $\text{cm}^{-1}$ ). The calculated oscillator strengths ( $f_{\text{cal}}$ ) from the ground state ( $\Psi J$ ) to the excited state ( $\Psi' J'$ ) can be calculated by Judd–Ofelt theory [22] from the equation

$$f_{\text{cal}} = \frac{8\pi^2 m c \nu}{3h(2J+1)} \times \frac{(n^2+2)^2}{9n} \sum_{\lambda=2,4,6} \Omega_{\lambda} |\langle \Psi J || U^{\lambda} || \Psi' J' \rangle|^2, \quad (12)$$

$$\Omega_{\lambda} = \frac{3h}{8\pi^2 m c} \times \frac{9n}{(n^2+2)^2} \times (2J+1) T_{\lambda}, \quad (13)$$

where  $h$  is the Planck's constant,  $J$  is the total angular momentum of the ground state,  $n$  is the refractive index of the samples,  $\nu$  is the energy of the transition,  $\Omega_{\lambda}$  ( $\lambda = 2, 4, 6$ ) are the Judd–Ofelt intensity parameter and  $||U^{\lambda}||^2$  is the square doubly reduced matrix element of the unit tensor. The Judd–Ofelt parameters  $\Omega_{\lambda}$  ( $\lambda = 2, 4, 6$ ) were calculated by using the least square fitting method between the experimental and calculated oscillator strengths and can be obtained using Eq. (14). In order to determine the accuracy of the obtained intensity parameters, the root-mean-square deviations ( $\delta_{\text{rms}}$ ) are calculated using the following relation:

$$\delta_{\text{rms}} = \left( \frac{\sum (f_{\text{cal}} - f_{\text{exp}})^2}{\sum f_{\text{exp}}^2} \right)^{1/2}, \quad (14)$$

where  $f_{\text{cal}}$  and  $f_{\text{exp}}$  are the calculated and experimental oscillator strengths, respectively, and the summation is

taken over all the bands used to evaluate  $\Omega_{\lambda}$ . The following radiative properties were also determined using Judd–Ofelt theory [23].

The spontaneous emission probability  $A_{\text{rad}}$  from ground state  $\Psi J$  to the excited state  $\Psi' J'$  for an electric dipole transition is given by

$$A_{\text{rad}} = \frac{64\pi^4 \nu^3 n(n^2+2)^2 e^2}{27hc^2(2J+1)} \times \sum_{\lambda=2,4,6} \Omega_{\lambda} |\langle \Psi J || U^{\lambda} || \Psi' J' \rangle|^2. \quad (15)$$

(a) The total radiative transition probability,  $A_T$ , obtained by carrying out the summation of all the transitions to the final states is given by

$$A_T = \sum A_{\text{rad}}. \quad (16)$$

(b) The values of  $A_{\text{rad}}$  and  $A_T$  can be used to calculate the fluorescence branching ratio  $\beta_r$ , given by

$$\beta_r = \frac{A_{\text{rad}}}{A_T}. \quad (17)$$

(c) The radiative lifetime of an emitting state is related to the total spontaneous emission probabilities for all transition which is represented by

$$\tau_{\text{rad}} = (A_T)^{-1}. \quad (18)$$

(d) The induced emission cross section  $\sigma$  for each transition is given by

$$\sigma = \frac{\lambda_p^4 A_{\text{rad}}}{8\pi c n^2 \Delta\lambda}, \quad (19)$$

where  $\lambda_p$  is the peak wavelength and  $\Delta\lambda$  is the full width at half maxima of the fluorescent peak for different transitions obtained from the emission spectra.

### 3. Results and discussion

#### 3.1. X-Ray Diffraction

The X-ray diffraction (XRD) patterns were recorded within the range of  $0^\circ \leq \theta \leq 100^\circ$ . The X-ray forms of the calcium sulfoborophosphate glasses, shown in Fig. 1, exhibited broad diffusion at lower scattering angles around  $5^\circ$ – $25^\circ$ , which explains the characteristics elongated range structural disorder that ascertain the amorphous nature of the prepared glasses [18].

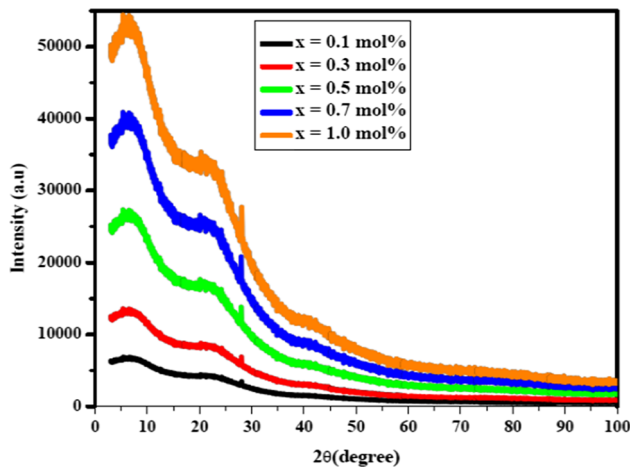


**Fig. 1** XRD pattern of  $25\text{CaSO}_4\text{-}30\text{B}_2\text{O}_3\text{-(}45\text{-}x\text{)P}_2\text{O}_5\text{-}x\text{Dy}_2\text{O}_3$  glasses

### 3.1.1. Infrared analysis

Figure 2 shows the IR spectra of  $25\text{CaSO}_4\text{-}30\text{B}_2\text{O}_3\text{-(}45\text{-}x\text{)P}_2\text{O}_5\text{-}x\text{Dy}_2\text{O}_3$  system with  $0.1 \leq x \leq 1.0$  (mol%). The band assignment and their corresponding vibrational positions are given in Table 1. The observed band's position between  $510$  and  $514\text{ cm}^{-1}$  frequency range is attributed to the bending vibrations of O–P–O bonds [24, 25]. Increasing the  $\text{Dy}_2\text{O}_3$  concentration and decreasing the  $\text{P}_2\text{O}_5$  concentration have resulted in broad and dissimilar stretching vibrations in the high-frequency bands. Any bands below  $600\text{ cm}^{-1}$  have significant aids from the modifier cations mostly present in the glass samples [26]. The band at  $670\text{ cm}^{-1}$  in  $Q^1$  structure corresponds to the bending mode of  $\text{PO}_4$  [27]. The band at  $705\text{-}721\text{ cm}^{-1}$  is assigned to the symmetric stretching

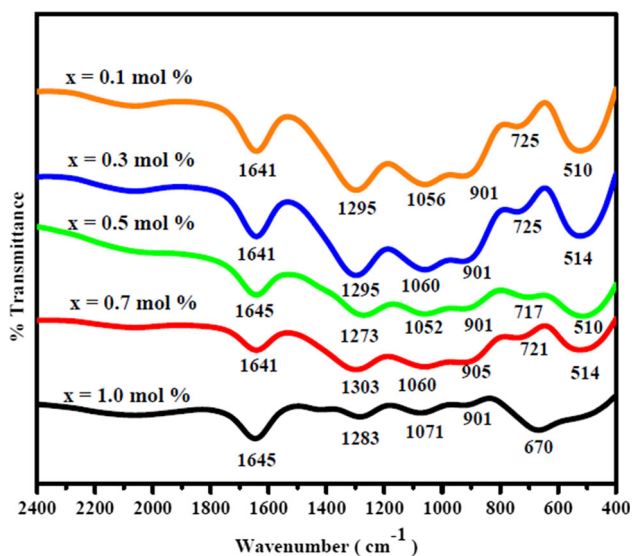


**Fig. 2** IR spectra of  $25\text{CaSO}_4\text{-}30\text{B}_2\text{O}_3\text{-(}45\text{-}x\text{)P}_2\text{O}_5\text{-}x\text{Dy}_2\text{O}_3$  glasses

vibrations of P–O–B linkages in the host and bending vibrations of B–O–B bonds [28]. The band at  $901\text{-}905\text{ cm}^{-1}$  belongs to the asymmetric vibrations  $V_{as}$  (P–O–P) of bridging oxygen atoms in phosphate chains [29]. The band around  $1056\text{-}1064\text{ cm}^{-1}$  is attributed to the symmetric stretching of P–O–B links between  $\text{BO}_4$  and  $\text{PO}_4$  groups [28]. The formation of B–O–P group bridged between P–O–P and B–O–B group decreased the  $\text{BO}_3$  units and increased the  $\text{BO}_4$  units in the network matrix and increased the NBOs in the glass host [28]. The band at  $1071\text{ cm}^{-1}$  is a combination of  $\nu(\text{SO}_4)$  and  $\nu(\text{BO}_4)$  [30]. The bands at  $1275\text{-}1303\text{ cm}^{-1}$  are assigned to boroxyl rings [31]. The bands at  $1641\text{-}1645\text{ cm}^{-1}$  are due to the change of  $\text{BO}_3$  units into  $\text{BO}_4$  units with NBOs in the glass host [28]. However, the intensity at  $1645\text{ cm}^{-1}$  increased, which indicates the creation of an additional number of P–O–P linkages and the decrease in the NBOs in the network.

### 3.2. Physical properties analysis

The physical properties given in Table 2 were calculated from some of the equations shown in Sects. 2.2.5 and 2.2.6. As illustrated in Fig. 3, the  $\text{Dy}^{3+}$  concentration is shown to vary with molar volume and density of sulfoborophosphate glasses, demonstrating an increase in density with increasing dysprosium ion concentration. A similar pattern was also observed for the average molecular weight of the prepared glasses. The increase in densities values may be due to an alteration in structural softening, coordination configuration and geometry, and the dimensional spaces of the prepared glass [32]. Meanwhile, the increase in molar volume could be due to a decrease in the bond length or inter-atomic spacing between the atoms that lead to the compactness of the network structure [33].

The resulting physical parameters of the  $\text{Dy}_2\text{O}_3$  glasses presented in Table 2 show that polaron radius decreases with increasing dysprosium ion concentration. The ion concentration was found to increase with increasing dysprosium ion content. This may be apparently due to an increase in ionic concentration of the dysprosium ion, which makes the field strength around dysprosium ions become high [34]. Furthermore, inter-ionic separation was found to decrease with increasing  $\text{Dy}^{3+}$  concentration, which eventually leads to more compactness of the sulfoborophosphate host of the prepared glass system.

### 3.3. Optical energy bandgap and Urbach's energy

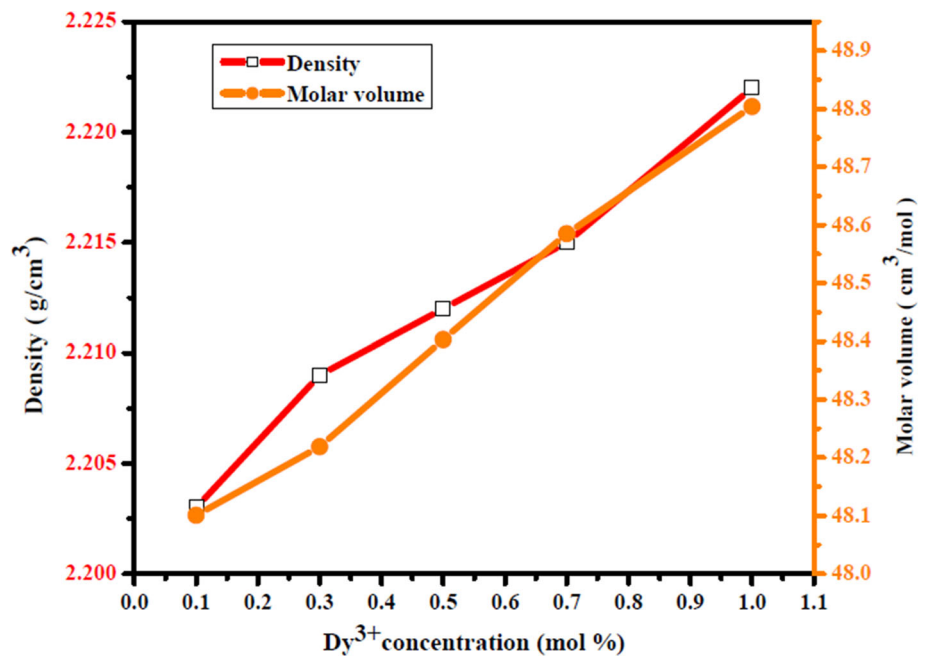
Table 3 shows the optical parameters of the prepared sulfoborophosphate glasses. Optical absorption spectra have been used to ascertain optical and Urbach's energy of the prepared glasses doped with dysprosium ions content. Values of indirect optical energy gap were determined by

**Table 1** IR band assignment and the reported values for  $25\text{CaSO}_4-30\text{B}_2\text{O}_3-(45-x)\text{P}_2\text{O}_5-x\text{Dy}_2\text{O}_3$  glasses

0.1 (mol%)	0.3 (mol%)	0.5 (mol%)	0.7 (mol%)	1.0 (mol%)	Reported values	Assignment
510	514	510	514	–	500–580	Bending vibrations of O–P–O
–	670	–	–	–	670	Bending vibration of $\text{PO}_4$ in $Q^1$
725	725	717	721	670	645–773	Combined B–O–B and P–O–P bonds
717					717	Stretching vibrations $V_s$ (P–O–P)
901	901	901	905	901	844–964	Asymmetric vibrations $V_{as}$ (P–O–P)
1056	1060	1052	1060	1071	1057	Symmetric stretching of P–O–B links
–	–	1071	–	–	1071	$\nu(\text{SO}_4)$ and $\nu(\text{BO}_4)$ .
1290	1281	1294	1272	1267	1240–1350	Boroxyl rings
1645	1645	1645	1645	1640	1647	Conversion of $\text{BO}_3$ units into $\text{BO}_4$ units

**Table 2** Physical parameters of  $25\text{CaSO}_4-30\text{B}_2\text{O}_3-(45-x)\text{P}_2\text{O}_5-x\text{Dy}_2\text{O}_3$  glasses

Physical parameters	Physical parameters for different $\text{Dy}_2\text{O}_3$ contents				
	X = 0.1 mol%	X = 0.3 mol%	X = 0.5 mol%	X = 0.7 mol%	X = 1.0 mol%
Average molecular weight $M_{av}$ (g)	105.96	106.51	107.06	107.61	108.44
Density, $\rho$ ( $\text{g cm}^{-3}$ )	2.203	2.209	2.212	2.215	2.222
Molar volume, $V_m$ ( $\text{cm}^3 \text{mol}^{-1}$ )	48.10	48.21	48.40	48.58	48.80
$\text{Dy}^{3+}$ ion concentration, $N_i$ ( $\times 10^{21}$ ions. $\text{s cm}^{-3}$ )	1.25	3.74	6.22	8.67	12.33
Polaron radius, $r_p$ ( $\times 10^{-8}$ Å)	3.80	2.63	2.22	1.99	1.77
Inter-ionic separation $r_i$ ( $\times 10^{-8}$ Å)	10.90	7.59	6.42	5.75	5.12
Field strength, $F$ ( $\times 10^{16}$ $\text{cm}^{-2}$ )	4.56	9.47	13.28	16.58	20.96

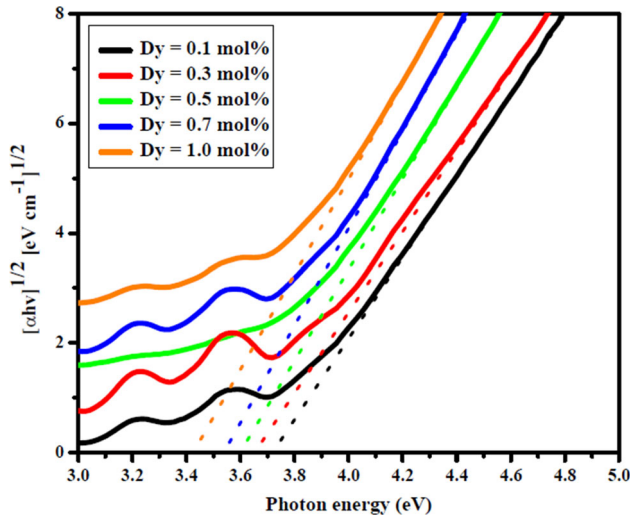
**Fig. 3** Variation of glass density and molar volume of  $25\text{CaSO}_4-30\text{B}_2\text{O}_3-(45-x)\text{P}_2\text{O}_5-x\text{Dy}_2\text{O}_3$  glasses

extrapolating the linear curve area of  $(\alpha h\nu)^{1/2}$  versus photon energy plot until it crosses the horizontal axis, with the intersect depicting the optical energy gap as shown in

Fig. 4. Thereafter, the same procedure was adapted to the linear curve region of the direct energy gap as illustrated in Fig. 5. The indirect and direct energy gap values obtained

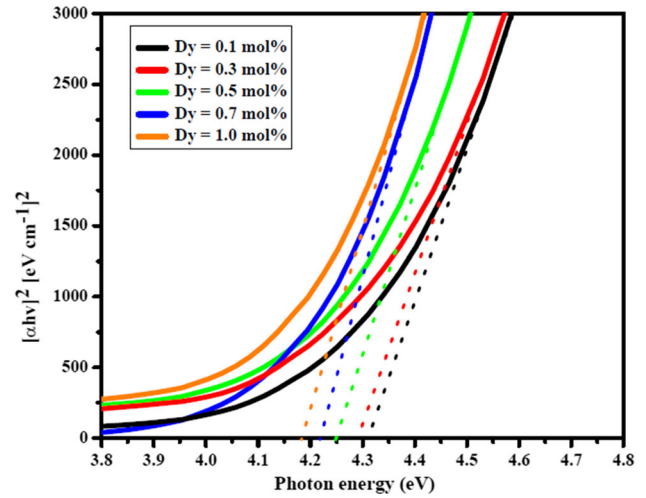
**Table 3** Optical parameters of 25CaSO<sub>4</sub>-30B<sub>2</sub>O<sub>3</sub>-(45-x)P<sub>2</sub>O<sub>5</sub>-xDy<sub>2</sub>O<sub>3</sub> glasses

Optical parameters	Optical parameters for different Dy <sub>2</sub> O <sub>3</sub> contents				
	0.1 mol%	0.3 mol%	0.5 mol%	0.7 mol%	1.0 mol%
Indirect energy gap (eV)	3.718	3.654	3.598	3.538	3.423
Direct energy gap (eV)	4.312	4.292	4.250	4.220	4.183
Urbach's energy (eV)	0.381	0.392	0.395	0.397	0.447
Refractive index	2.227	2.240	2.252	2.266	2.292
Dielectric constant	4.959	5.018	5.072	5.135	5.251
Optical dielectric constant	3.959	4.018	4.072	4.135	4.251
Reflection losses	0.145	0.146	0.148	0.150	0.154
Molar refractivity (cm <sup>3</sup> mol <sup>-1</sup> )	27.365	27.601	27.870	28.157	28.612
Electron polarizability (Å <sup>3</sup> )	10.859	10.953	11.059	11.173	11.354

**Fig. 4** Tauc's plot of  $(\alpha hv)^{1/2}$  as a function of photon energy of 25CaSO<sub>4</sub>-30B<sub>2</sub>O<sub>3</sub>-(45-x)P<sub>2</sub>O<sub>5</sub>-xDy<sub>2</sub>O<sub>3</sub> glasses

were in the range 3.718–3.423 and 4.183–4.312 eV, respectively, showing a continuous decrease with increasing dysprosium ion concentration. Such decrease may be attributed to the structural changes and creation of NBOs, which resulted in the formation of bonding defects in network matrix of the prepared glasses. However, the values of direct and indirect energy gap obtained in this study are higher than earlier reported values [18] (Fig. 6).

Similarly, values of Urbach's energy obtained using Eq. 2 are given in Table 3, which increase unceasingly with increasing dysprosium ion concentration. The glass with higher dysprosium ion concentration possesses the highest value of Urbach's energy, and this is an indication of the likelihood of elongated range order locally arising from the bonding defects; these defects yield localized states in the glasses inflicting the decrease in the width of the localized states in the optical energy gap. The Urbach's

**Fig. 5** Tauc's plot of  $(\alpha hv)^2$  as a function of photon energy of 25CaSO<sub>4</sub>-30B<sub>2</sub>O<sub>3</sub>-(45-x)P<sub>2</sub>O<sub>5</sub>-xDy<sub>2</sub>O<sub>3</sub> glasses

energy also gives information about the degree of compactness and dis-orderness in amorphous material. Hence, these values are consistent with previous studies [18, 35].

The refractive index and molar refraction are important properties in optical glasses and are closely related to polarization properties. It was observed that an increase in dysprosium ions content apparently increased the refractive index and molar refraction, which in turn increases the electron polarizability as given in Table 3. Therefore, from the value of the refractive index, other essential parameters were calculated, which include dielectric constant, optical dielectric constant and reflection loss from the glass surface, and all these parameters are found to be increasing with increasing dysprosium ions content.

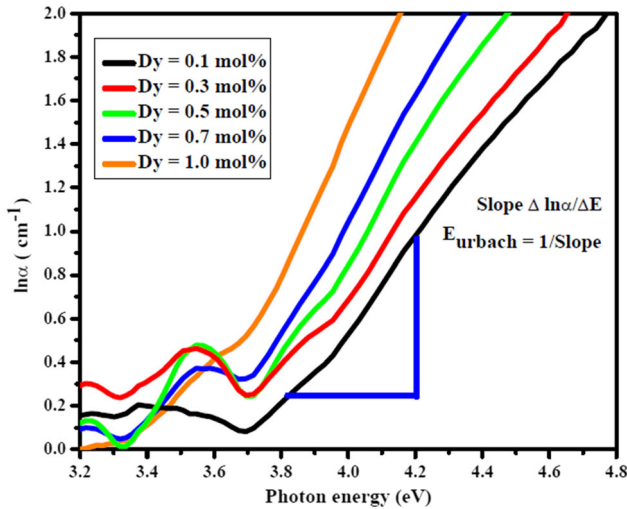


**Fig. 6** Graph of  $\ln\alpha$  as a function of photon energy to determine the  $E_{\text{urb}}$  of  $25\text{CaSO}_4\text{-}30\text{B}_2\text{O}_3\text{-(}45\text{-}x\text{)P}_2\text{O}_5\text{-}xDy_2\text{O}_3$  glasses

### 3.4. Spectral Absorption Analysis

The spectral absorption of the sulfoborophosphate glasses doped with dysprosium ions was recorded in the spectral ranges of 300–2100 nm as displayed in Fig. 7. The spectrum displays nine broadened absorption peaks centered at 351, 383, 451, 752, 799, 896, 1090, 1269 and 1670 (in nm) corresponding to the ground-state transitions  ${}^6\text{H}_{15/2}$  to the excited states of  ${}^6\text{P}_{7/2}$ ,  ${}^4\text{F}_{7/2}$ ,  ${}^4\text{I}_{15/2}$ ,  ${}^6\text{F}_{3/2}$ ,  ${}^6\text{F}_{5/2}$ ,  ${}^6\text{F}_{7/2}$ ,  ${}^6\text{F}_{9/2}$ ,  ${}^6\text{F}_{11/2}$  and  ${}^4\text{H}_{11/2}$ . Additionally, absorption band monitored at 1269 nm belongs to the oversensitive transition ( ${}^6\text{H}_{15/2} \rightarrow {}^6\text{F}_{11/2}$ ) that possesses the uppermost intensity when compared with other transitions. This indicates that it follows the selection rules, i.e., to each rare earth ion, the spectral intensities and the positions of some absorption

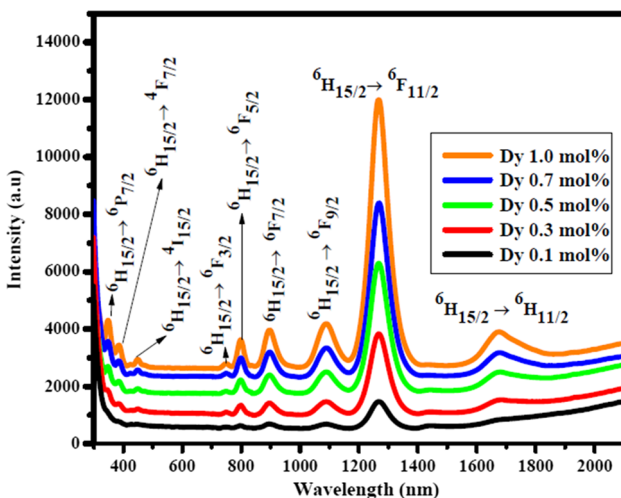


**Fig. 7** Absorption spectra of  $25\text{CaSO}_4\text{-}30\text{B}_2\text{O}_3\text{-(}45\text{-}x\text{)P}_2\text{O}_5\text{-}xDy_2\text{O}_3$  glasses

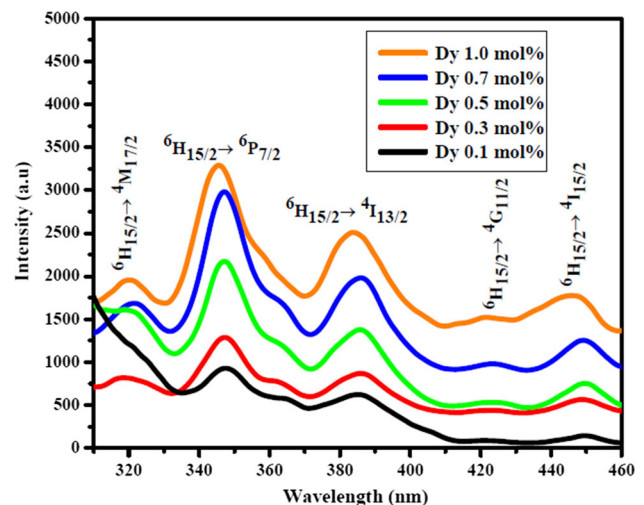
transitions are sensitive to the environment around the rare earth [35, 36].

### 3.5. Excitation Spectra Analysis

Figure 8 shows the excitation spectra of sulfoborophosphate glasses doped with dysprosium ions that were recorded in the range of 310–460 nm wavelength. The spectrum excitation for 572 nm emission displayed five distinct bands at 319 nm, 345 nm, 383 nm, 421 nm and 446 nm that correspond to the ground-state transitions  ${}^6\text{H}_{15/2}$  to the excited states of  ${}^4\text{M}_{7/2}$ ,  ${}^6\text{P}_{7/2}$ ,  ${}^4\text{I}_{13/2}$ ,  ${}^4\text{G}_{11/2}$  and  ${}^4\text{I}_{15/2}$  levels. Upon all the various excited bands, the band  ${}^6\text{H}_{15/2} \rightarrow {}^6\text{P}_{7/2}$  at 345 nm appeared to be the most intense one which happened to be the excitation wavelength. It was observed that the calcium sulfoborophosphate glasses doped with dysprosium could be excited by UV radiation [37].

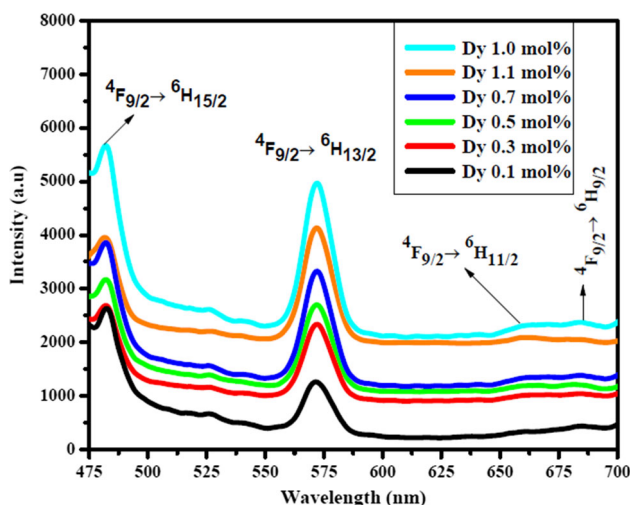
### 3.6. Emission Spectra Analysis

Figure 9 depicts the spectral emission of sulfoborophosphate glasses doped with different concentrations of dysprosium ion. The emission spectra have been recorded and obtained by monitoring emission within the range of 475–625 nm due to an excitation wavelength of 345 nm. The spectrum displays two intense bands at 482 and 572 nm, corresponding to  ${}^4\text{F}_{9/2} \rightarrow {}^6\text{H}_{15/2}$  (blue) and  ${}^4\text{F}_{9/2} \rightarrow {}^6\text{H}_{13/2}$  (yellow), and two weak bands at 661 nm ( ${}^4\text{F}_{9/2} \rightarrow {}^6\text{H}_{11/2}$ ) and 684 nm ( ${}^4\text{F}_{9/2} \rightarrow {}^6\text{H}_{9/2}$ ). Figure 9 shows that the magnetic dipole transition possesses higher strength compared with the allowed electric dipole transition, which is an indication of a high symmetry around the dysprosium ions in the existing glass [38]. It was also



**Fig. 8** Excitation spectra of  $25\text{CaSO}_4\text{-}30\text{B}_2\text{O}_3\text{-(}45\text{-}x\text{)P}_2\text{O}_5\text{-}xDy_2\text{O}_3$  glasses





**Fig. 9** Emission spectra of 25CaSO<sub>4</sub>-30B<sub>2</sub>O<sub>3</sub>-(45-x)P<sub>2</sub>O<sub>5</sub>-xDy<sub>2</sub>O<sub>3</sub> glasses

**Table 4** Spectral properties of Dy<sup>3+</sup>

Dy <sup>3+</sup> concentration (mol%)	Luminescence intensity (a.u.)		Y/B
	<sup>4</sup> F <sub>9/2</sub> → <sup>6</sup> H <sub>15/2</sub> blue	<sup>4</sup> F <sub>9/2</sub> → <sup>6</sup> H <sub>13/2</sub> yellow	
0.1	5709.91	4925.43	0.86
0.3	3926.79	3916.23	0.99
0.5	3808.79	3260.31	0.85
0.7	3164.16	2692.16	0.85
1.0	2731.49	2361.01	0.86
1.1	2576.34	1243.37	0.48

observed that the emission intensities increased with increasing dysprosium ion concentrations.

Table 4 shows the luminescence intensities of the intense transitions and Y/B values of dysprosium ion. The resulting values of Y/B intensity ratios for all the glasses were found to be less than unity, which may be attributed to the lower degree of covalency [34]. It was apparent that the variation in Y/B intensity ratio values with dysprosium concentration clearly signifies the change in coordination of dysprosium ion. Thus, the luminescence intensity attained maximum value at 1.0 mol% dysprosium ion concentration, which subsequently decreases due to concentration quenching.

### 3.7. Nephelauxetic ratio and bonding parameter

Figure 10 illustrates the average nephelauxetic ratios ( $\beta$ ) and the bonding parameters ( $\delta$ ) of sulfoborophosphate glasses doped with different concentrations of dysprosium ion. Nephelauxetic ratios ( $\beta$ ) and the bonding parameters

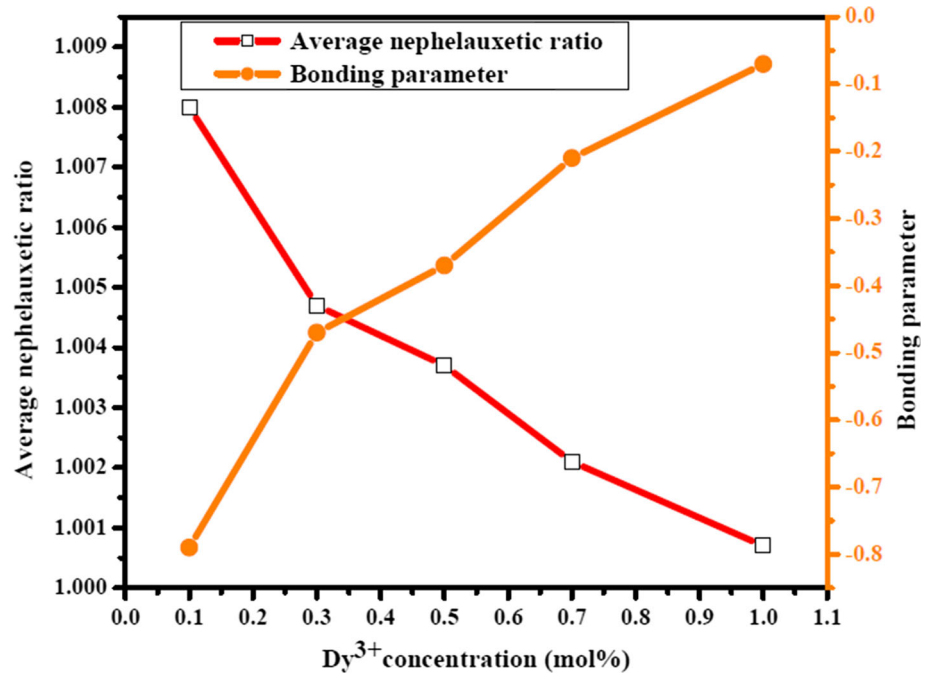
( $\delta$ ) are the bonding characteristics determined from the bond positions (cm<sup>-1</sup>) of the spectral absorption. Table 5 depicts the values of nephelauxetic ratios ( $\beta$ ) calculated using the expression  $\beta = (V_c/V_a)$ , where  $V_c$  is the transition wavenumber (in cm<sup>-1</sup>) of the dysprosium ion and  $V_a$  expresses the wavenumber (in cm<sup>-1</sup>) of the exact transition for aquo ion reported by Carnall et al [39]. The average nephelauxetic ratios ( $\bar{\beta}$ ) were determined by dividing values of  $\beta$  to the total number of energy positions, while values of the bonding parameter were obtained using the expression  $\delta = (1 - \bar{\beta}/\beta) \times 100$ . The metal ligand band could be covalent or ionic depending upon the positive or negative values of the  $\delta$ . The negative sign of  $\delta$  in this report indicates that the bonding between Dy<sup>3+</sup> ions and the surrounding ligands is ionic in nature. Decreasing the values of  $\bar{\beta}$  indicates an increase in covalence character of the glasses [40]

The calculated and experimental oscillator strengths of Dy<sup>3+</sup> ion-doped 25CaSO<sub>4</sub>-30B<sub>2</sub>O<sub>3</sub>-(45-x)P<sub>2</sub>O<sub>5</sub>-xDy<sub>2</sub>O<sub>3</sub> glasses are displayed in Table 6. It is clear that both calculated and experimental oscillator strengths attained optimum value at <sup>6</sup>H<sub>15/2</sub> → <sup>6</sup>F<sub>11/2</sub> transition. This is because of hypersensitivity transition that usually has the maximum intensity in the spectra. The fitting quality is obtained from the root-mean-square deviation as given in Table 6, which is in good agreement with earlier reported values [41]. The deviation sufficiently demonstrates acceptable fitting between experimental and calculated oscillator strengths, which obeys the Judd-Ofelt theory.

Intensity parameters  $\Omega_\lambda$  ( $\lambda = 2, 4$  and  $6$ ) for the glasses doped with Dy<sub>2</sub>O<sub>3</sub> are displayed in Table 7.  $\Omega_\lambda$  values of all the glasses were in the order of  $\Omega_2 > \Omega_4 > \Omega_6$ , which are consistent with previous studies [4, 41–43]. Among the three J-O parameters,  $\Omega_2$  is related to the covalency and structural changes near the dysprosium ion described as short-range effects, while  $\Omega_4$  and  $\Omega_6$  are related to the rigidity and viscosity and are strongly influenced by vibrational levels associated with the central rare earth ions bound to the ligand atoms [43].

Following the use of Judd-Ofelt theory to determine  $\Omega_2$ ,  $\Omega_4$  and  $\Omega_6$  parameters, further evaluations were performed to estimate the radiative transition probabilities ( $A_{rad}$ ), radiative lifetimes of excited states ( $\tau_{rad}$ ), fluorescence branching ratios ( $\beta_r$ ) and emission cross section ( $\sigma$ ), which are presented in Table 8. The values of radiative transition probability ( $A_{rad}$ ) for <sup>4</sup>F<sub>9/2</sub> → <sup>6</sup>H<sub>13/2</sub> were found to be higher compared with <sup>4</sup>F<sub>9/2</sub> → <sup>6</sup>H<sub>15/2</sub> transitions, which increase with increasing Dy<sup>3+</sup> ion concentration. The previous studies have shown that emission transition having branching ratio higher than 50% is considered suitable for laser emission [41, 44]. The high branching ratio of more than 50% observed in <sup>4</sup>F<sub>9/2</sub> → <sup>6</sup>H<sub>13/2</sub> is a good indicative to be regarded as lasing transition. Large

**Fig. 10** Variation of average nephelauxetic ratio and bonding parameter of  $25\text{CaSO}_4-30\text{B}_2\text{O}_3-(45-x)\text{P}_2\text{O}_5-x\text{Dy}_2\text{O}_3$  glasses



stimulated emission cross section is an attractive feature for low-threshold, high-gain laser application, which is utilized to obtain a continuous-wave laser action [44]. As illustrated in Table 8, the  ${}^4\text{F}_{9/2} \rightarrow {}^6\text{H}_{13/2}$  transition has the highest emission cross-sectional values for the two observed transitions.

Furthermore, glass formation with a mixture of  $\text{SO}_4$  and  $\text{P}_2\text{O}_5$  is possible only if the phosphate network contains  $[\text{POO}_{2/2}\text{O}]^-$  and  $[\text{POO}_{1/2}\text{O}_2]^{-1}$  structural groups [45, 47]. Similarly, glass formation of dithiophosphate species is possible when sulfate and  $[\text{POO}_{2/2}\text{O}]^-$  ions are present simultaneously. The concentration of such species relies on

the nature of the modifier ion which usually affects rare earth emission probabilities [46]. Furthermore, varying concentrations of phosphate structural units, sulfate ions as well as their linkages are expected to alter the crystal field around the lanthanide ions in glass network [47].

#### 4. Conclusions

Calcium sulfoborophosphate mixed with different contents of dysprosium ions has been successfully synthesized by a convectional melt-quenching technique. The amorphous

**Table 5** Nephelauxetic ratio of  $25\text{CaSO}_4-30\text{B}_2\text{O}_3-(45-x)\text{P}_2\text{O}_5-x\text{Dy}_2\text{O}_3$  glasses

Transitions ${}^6\text{H}_{15/2} \rightarrow$	Nephelauxetic ratio ( $\beta$ ) for different $\text{Dy}_2\text{O}_3$ contents					Aqueous ions band position ( $\text{cm}^{-1}$ ) [32]
	0.1 mol%	0.3 mol%	0.5 mol%	0.7 mol%	1.0 mol%	
${}^6\text{P}_{7/2}$	1.0037	1.0134	1.0031	1.0054	0.9855	28,551
${}^4\text{F}_{7/2}$	0.9946	0.9782	0.9782	0.9782	0.9760	26,341
${}^4\text{I}_{15/2}$	1.0031	0.9954	0.9916	0.9891	0.9957	22,293
${}^6\text{F}_{3/2}$	0.9996	0.9985	0.9985	0.9996	0.9985	13,250
${}^6\text{F}_{5/2}$	1.0119	1.0039	1.0083	0.9995	1.0039	12,432
${}^6\text{F}_{7/2}$	1.0079	1.0079	1.0079	1.0119	1.0081	11,025
${}^6\text{F}_{9/2}$	1.0058	1.0097	1.0097	1.0107	1.0097	9087
${}^6\text{F}_{11/2}$	1.0186	1.0160	1.0186	1.0108	1.0160	7730
${}^6\text{H}_{11/2}$	1.0186	1.0127	1.0118	1.0111	1.0107	5833
$\bar{\beta}$	1.0070	1.0040	1.0031	1.0018	1.0005	1
$\Delta$	- 0.70	- 0.40	- 0.31	- 0.18	- 0.05	0

**Table 6** Experimental and calculated oscillator field strengths ( $\times 10^{-6}$ ) and root-mean-square deviation ( $\delta_{\text{rms}}$ ) for 25CaSO<sub>4</sub>–30B<sub>2</sub>O<sub>3</sub>–(45– $x$ )P<sub>2</sub>O<sub>5</sub>– $x$ Dy<sub>2</sub>O<sub>3</sub> with  $0.1 \leq y \leq 1.0$  mol% glasses

Transition	0.1 mol%		0.3 mol%		0.5 mol%		0.7 mol%		1.0 mol%	
	$f_{\text{exp}}$	$f_{\text{cal}}$	$f_{\text{exp}}$	$f_{\text{cal}}$	$f_{\text{exp}}$	$f_{\text{cal}}$	$f_{\text{exp}}$	$f_{\text{cal}}$	$f_{\text{exp}}$	$f_{\text{cal}}$
${}^6\text{H}_{15/2} \rightarrow {}^6\text{F}_{3/2}$	–	–	–	–	–	–	–	–	1.07	0.25
${}^6\text{H}_{15/2} \rightarrow {}^6\text{F}_{5/2}$	1.07	0.28	2.47	0.39	3.18	0.74	3.05	1.04	2.84	1.25
${}^6\text{H}_{15/2} \rightarrow {}^6\text{F}_{7/2}$	2.54	1.44	3.43	2.19	4.04	3.37	4.39	3.10	4.26	3.81
${}^6\text{H}_{15/2} \rightarrow {}^6\text{F}_{9/2}$	3.73	3.92	4.38	5.13	6.16	6.72	5.65	5.96	6.13	4.13
${}^6\text{H}_{15/2} \rightarrow {}^6\text{F}_{11/2}$	14.18	14.01	17.12	17.03	18.78	18.67	19.52	19.76	19.82	19.85
${}^6\text{H}_{15/2} \rightarrow {}^6\text{H}_{11/2}$	–	–	1.13	1.44	1.31	1.97	1.624	2.03	2.14	2.18
$\delta_{\text{rms}}$	$\pm 0.10$		$\pm 0.14$		$\pm 0.13$		$\pm 0.11$		$\pm 0.12$	

**Table 7** Judd–Ofelt intensity parameters  $\Omega_2$ ,  $\Omega_4$  and  $\Omega_6$  ( $\times 10^{-20}$ ) of the 25CaSO<sub>4</sub>–30B<sub>2</sub>O<sub>3</sub>–(45– $x$ )P<sub>2</sub>O<sub>5</sub>– $x$ Dy<sub>2</sub>O<sub>3</sub> with ( $0.1 \leq y \leq 1.0$  mol%) glasses

$Y$ mol Dy <sup>3+</sup> %	$\Omega_2$	$\Omega_4$	$\Omega_6$	Trend	$\Omega_4/\Omega_6$
0.1	5.63	2.15	0.44	$\Omega_2 > \Omega_4 > \Omega_6$	4.88
0.3	7.85	3.24	0.51	$\Omega_2 > \Omega_4 > \Omega_6$	6.35
0.5	9.03	4.12	0.57	$\Omega_2 > \Omega_4 > \Omega_6$	7.22
0.7	9.16	5.02	1.13	$\Omega_2 > \Omega_4 > \Omega_6$	4.44
1.0	10.71	4.23	1.22	$\Omega_2 > \Omega_4 > \Omega_6$	3.46

nature of the glass samples was determined by X-ray diffraction. It can be deduced that an increase in dysprosium ion gave rise to the formation of NBOs by infrared. In this present work, the optical properties and spectroscopic attributes of the Dy<sup>3+</sup>-doped calcium sulfoborophosphate glasses were characterized by absorption, excitation and emission measurements. The replacement of P<sub>2</sub>O<sub>3</sub> with Dy<sub>2</sub>O<sub>3</sub> improves the nonlinearity of the present glass samples. The emission spectra demonstrated two

prominent emission bands at 482 nm ( ${}^4\text{F}_{9/2} \rightarrow {}^6\text{H}_{15/2}$ ) and 572 nm ( ${}^4\text{F}_{9/2} \rightarrow {}^6\text{H}_{13/2}$ ) and two feeble bands at 661 nm ( ${}^4\text{F}_{9/2} \rightarrow {}^6\text{H}_{11/2}$ ) and 684 nm ( ${}^4\text{F}_{9/2} \rightarrow {}^6\text{H}_{9/2}$ ). The negative values of the bonding parameters confirmed the ionic nature of dysprosium ions–ligand bond in the network matrix. The validity of the Judd–Ofelt and benefit of fitting procedure have been manifested owing to the low root-mean-square deviation between the experimental and calculated oscillator strengths. The  $\Omega_2$  and Y/B ratio values of the present glasses showed that dysprosium ions were situated in a high-asymmetry glass network environment. The  ${}^4\text{F}_{9/2} \rightarrow {}^6\text{H}_{13/2}$  emission band affirmed to possessing higher branching ratio and stimulated cross section. The result of the bandgap energy, the nonlinearity graphs presented, excellent structural features shown by Fourier transform infrared analysis, excellent photoluminescence displayed, and higher value of branching ratio and stimulated cross section demonstrated by the present glasses amplify their suitability for solid-state lasers, nonlinear optical amplifier and white LED's applications.

**Table 8** Emission band position ( $\lambda_p$ , nm), radiative transition probability ( $A_{\text{rad}}$ , s<sup>–1</sup>), total radiative transition probability ( $A_{\text{T}}$ ), fluorescence branching ratio ( $\beta_r$ , %), calculated lifetime ( $\tau_{\text{cal}} \times 10^{-4}$ ) and emission cross section ( $\sigma \times 10^{-22}$ ) (cm<sup>2</sup>) for 25CaSO<sub>4</sub>–30B<sub>2</sub>O<sub>3</sub>–(45– $x$ )P<sub>2</sub>O<sub>5</sub>– $x$ Dy<sub>2</sub>O<sub>3</sub> glasses

Transition	Parameter	0.1 mol%	0.3 mol%	0.5 mol%	0.7 mol%	1.0 mol%	1.1 mol%
${}^4\text{F}_{9/2} \rightarrow {}^6\text{H}_{15/2}$	$\lambda_p$	482	482	481	482	482	481
	$A_{\text{rad}}$	538.12	660.32	1074.52	1126.17	1232.43	1363.62
	$\beta_r$	10.0	10.0	13.0	13.0	13.0	14.0
	$\sigma$	7.97	3.98	2.65	1.99	1.59	1.32
${}^4\text{F}_{9/2} \rightarrow {}^6\text{H}_{13/2}$	$\lambda_p$	572	572	572	571	572	572
	$A_{\text{rad}}$	4795.13	5863.05	6615.63	7271.48	8113.66	8345.61
	$\beta_r$	89.0	89.0	86.0	86.0	86.0	85.0
	$\sigma$	72.23	74.13	82.54	85.32	48.4	22.82
	$A_{\text{T}}$	5333.25	6523.37	7690.15	8397.65	9346.09	9709.23
	$\tau_{\text{cal}}$ (ms)	1.87	1.53	1.30	1.19	1.06	1.02

**Acknowledgements** We thank the Ministry of Higher Education Malaysia (MOHE) and UTM for giving us financial assistance through the Fundamental Research Grant Scheme (FRGS), Vote Number (Q. J130000.2526.16H24).

## References

- [1] V R Prasad, S Damodaraiah, M Seshadri, S Babu and Y C Ratnakaram *Indian J Phys.* **91** 1265 (2017)
- [2] S Selvi, G Venkataiah, S Arunkumar, G Muralidharan and K Marimuthu *Phys. B: Condens. Matter.* **454** 72 (2014)
- [3] V Simon, D Muresan, A F Takács, M Neumann and S Simon *Solid State Ionics.* **178** 221 (2007)
- [4] S S Babu, P Babu, C K Jayasankar, W Sievers, T Tröster and G Wortmann *J. Lumin.* **126** 109 (2007)
- [5] V B Sreedhar, D Ramachari, and C K Jayasankar *Phys. B: Condens. Matter.* **408** 158 (2013)
- [6] P Babu and C K Jayasankar *Opt. Mater.* **15** 65 (2000)
- [7] S Jiang *et al. J. Non-cryst. Solids.* **263** 364 (2000)
- [8] M H Wan, P S Wong, R Hussin, H O Lintan, and S Endud *Spectrosc. Lett.* **48** 473 (2015)
- [9] D Rajesh, A Balakrishna and Y C Ratnakaram *Opt. Mater.* **35** 108 (2012)
- [10] P Mošner, K Vosejpková, L Koudelka, L Montagne and B Revel *J. Non-Cryst. Solids.* **357** 2648 (2011)
- [11] R Yang *et al. J. Alloys Compd.* **513** 97 (2012)
- [12] X Li, H Yang, X Song and Y Wu *J. Non-Cryst. Solids.* **379** 208 (2013)
- [13] M S Gaafar, S Y Marzouk, H A Zayed, L I Soliman and A S El-Deen *Curr. Appl. Phys.* **13** 152 (2013)
- [14] R Stefan, P Pascuta, A Popa, O Raita, E Indrea and E Culea *J. Phys. Chem. Solids.* **73** 221 (2012)
- [15] I m Sang Hyeok, Y H Na, N J Kim, D H Kim, C W Hwang and B K Ryu *Thin Solid Films.* **518** e46 (2010)
- [16] F H ElBatal, S Ibrahim and A M Abdelghany *J. Mol. Struct.* **1030** 107 (2012)
- [17] L Koudelka, P Mošner and J Šubčík *IOP Conf. Ser. Mater. Sci. Eng.* **2** 012015 (2009)
- [18] I Bulus, S A Dalhatu, R Hussin, W N Wan Shamsuri and Y A Yamusa *Int. J. Mod. Phys. B.* **31** 1750101 (2017)
- [19] T Inoue, T Honma, V Dimitrov and T Komatsu *J. Solid State Chem.* **183** 3078 (2010)
- [20] Y M Lai, X F Liang, S Y Yang, J X Wang and B T Zhang *J. Mol. Struct.* **1013** 134 (2012)
- [21] I Kindrat, B Padlyak and A Drzewiecki *J. Luminesc.* **166** 264 (2015)
- [22] Y A Yamusaa, R Hussin, W N Wan Shamsuri, Y A Tanko and S A Jupri *Optik.* **164** 324 (2018)
- [23] Y A Yamusa, R Hussin, W N Wan Shamsuri *Chin. J. Phys.* **56** 932 (2018)
- [24] R Stefan and M Karabulut *J. Mol. Struct.* **1071** 45 (2014)
- [25] M H Wan, P S Wong, R Hussin, H O Lintang and S Endud *J. Alloys Compd.* **595** 39 (2014)
- [26] M A Ouis, A M Abdelghany and H A ElBatal *Process. Appl. Ceram.* **6** 141 (2012)
- [27] D Shajan, P Murugasen and S Sagadevan *Optik Int. J. Light Electron Opt.* **136** 165 (2017)
- [28] M Vijayakumar, and K Marimuthu *J. Alloys Compd.* **629** 230 (2015)
- [29] A R Kumar, C S Rao, N N Rao, V R Kumar, I V Kityk and N Veeraiah *J. Non-Cryst. Solids.* **358** 1278 (2012)
- [30] M Daub, H A Höpfe and H Hillebrecht *Zeitschrift für anorganische und allgemeine Chemie.* **640** 2914 (2014)
- [31] M Rada, S Rada, P Pascuta and E Culea *Spectrochim. Acta Part A Mol. Biomol. Spectrosc.* **77** 832 (2010)
- [32] S F Khor, Z A Talib and W M Yunus *Ceram. Int.* **38** 935 (2012)
- [33] T. Rao *et al. Spectrochim. Acta A. Mol. Biomol. Spectrosc.* **118** 744 (2014).
- [34] S A Azizan, S Hashim, N A Razak, M H A Mhareb, Y S M Alajerami and N Tamchek *J. Mol. Struct.* **1076** 20 (2014)
- [35] M H A Mhareb *et al. J. Luminesc.* **177** 366 (2016)
- [36] Y S M Alajerami, S Hashim, W M S W Hassan, A T Ramli and A Kasim *Phys. B Condens. Matter.* **407** 2398 (2012)
- [37] K Swapna, S Mahamuda, A S Rao, M Jayasimhadri, T Sasikala and L R Moorthy *J. Luminesc.* **139** 119 (2013)
- [38] A Balakrishna, D Rajesh and Y C Ratnakaram *J. Luminesc.* **132** 2984 (2012)
- [39] W T Carnall, P R Fields and K Rajnak *J. Chem. Phys.* **49** 4412 (1968)
- [40] V Uma, K Maheshvaran, K Marimuthu and G Muralidharan *Struct. J. Luminesc.* **176** 15 (2016)
- [41] M Vijayakumar, K Mahesvaran, D K Patel, S Arunkumar and K Marimuthu *Opt. Mater.* **37** 695 (2014)
- [42] B C Jamalayah, L R Moorthy and H J Seo *J. Non-Cryst. Solids* **358** 204 (2012)
- [43] F Ahmadi, R Hussin and S K Ghoshal *J. Non-Cryst. Solids* **452** 266 (2016)
- [44] K S Lim, N Vijaya, C R Kesavulu and C K Jayasankar *Opt. Mater.* **35** 1557 (2013)
- [45] F Ahmadi, R Hussin and S K Ghoshal *J. Non-Cryst. Solids* **448** 43 (2016)
- [46] P R Rao, N Venkatramaiah, Y Gandhi, V R Kumar, I V Kityk and N Veeraiah *Spectrochim. Acta Part A Mol. Biomol. Spectrosc.* **86** 472 (2012)
- [47] P R Rao, G M Krishna, M G Brik, Y Gandhi and N Veeraiah *J. Luminesc.* **131** 212 (2011)